https://doi.org/10.5194/egusphere-2026-4968
Preprint. Discussion started: 11 September 2026


# Representativeness of TROPOMI tropospheric $NO_2$ columns near Asian airports constrained by IAGOS airborne measurements

Hyunkwang Lim[1], Tamaki Fujinawa[1], Takafumi Sugita[1], Satoshi Inomata[1], Hiroshi Tanimoto[1], Christoph Mahnke[2], Andreas Petzold[2], Ulrich Bundke[2], Yugo Kanaya[3], Yasuko Kasai[4], Tomohiro Sato[4], Sang Seo Park[5], Minseok Kim[5,6], Yun Gon Lee[7], Ukkyo Jeong[8]

[1] Earth System Division, National Institute of Environmental Studies, Ibariki 305-8506, Japan
[2] Forschungszentrum Jülich GmbH (FZJ), Institute of Climate and Energy Systems: Troposphere (ICE-3), Jülich 52428, Germany
[3] Earth Surface System Research Center, Japan Agency for Marine-Earth Science and Technology, Kanagawa, 236-0001, Japan
[4] Terahertz Technology Research Center, National Institute of Information and Communications Technology, Tokyo, 184-8795, Japan
[5] Department of Civil, Urban, Earth, and Environmental Engineering, Ulsan National Institute of Science and Technology, Ulsan, 44919, Republic of Korea
[6] AI-Transformed Aerospace InnoCORE Research Center, Korea Advanced Institute of Science and Technology, (KAIST), Daejeon 34141, Republic of Korea
[7] Department of Earth, Environmental & Space Sciences, Chungnam National University, Daejeon 34134, Republic of Korea
[8] Division of Earth Environmental System Science, Major of Spatial Information Engineering, Pukyong National University, Pusan, 48513, Republic of Korea

*Correspondence to*: Hyunkwang Lim (lim.hyunkwang@nies.go.jp) and Hiroshi Tanimoto (tanimoto@nies.go.jp)

**Abstract.** Tropospheric $NO_2$ data retrievals from the satellite-borne TROPOspheric Monitoring Instrument (TROPOMI) are sensitive to the vertical profile assumed in the air mass factor (AMF) calculation, especially in polluted lower-tropospheric environments. This study investigated the use of aircraft and ground-based profile information to evaluate this sensitivity near five major airports. We combined TROPOMI tropospheric $NO_2$ vertical column densities (VCDs), land-based Pandora observations, and airplane-based In-service Aircraft for a Global Observing System (IAGOS) descent profiles for selected airport–Pandora pairs in Japan, South Korea, and Thailand from March to July 2025. Before applying profile-based AMF recalculations, we examined whether the TROPOMI $NO_2$ field around each Pandora site was representative of that around the corresponding airport. The airport- and Pandora-region time series were generally coherent, although their mean $NO_2$ levels differed, indicating that temporal consistency and absolute spatial representativeness need to be considered separately.

The lower part of the a priori $NO_2$ profile obtained by the TM5-MP model was then replaced with IAGOS-derived profiles to recalculate TROPOMI AMFs and VCDs. The IAGOS-profile recalculation reduced the overall low bias relative to Pandora data and improved several validation metrics, but the response differed by site. Improvements were most evident where the

https://doi.org/10.5194/egusphere-2026-4968
Preprint. Discussion started: 11 September 2026


IAGOS descent profiles, Pandora site, and satellite-observed $NO_2$ field sampled similar environments. In contrast, weaker or degraded performance occurred when the aircraft profiles represented an air mass different from that influencing the Pandora-acquired column. The Pandora-scaled-profile case produced the closest agreement with Pandora results, but the comparison is more suitable as a profile-sensitivity test rather than an independent validation. Residual diagnosis showed that the remaining differences after the Pandora-scaled-profile recalculation were not mainly controlled by horizontal $NO_2$ heterogeneity, pixel sampling density, mean quality assurance value, or the magnitude of the AMF correction. A slant column density (SCD)-equivalent closure analysis further suggested that profile replacement alone cannot fully reconcile TROPOMI and Pandora columns, because the recalculated VCD still depends on the TROPOMI effective tropospheric SCD and other non-profile retrieval inputs. These findings demonstrate the value of IAGOS and Pandora lower-tropospheric profile information for diagnosing TROPOMI $NO_2$ AMF uncertainty near airports, while underscoring the need to account for slant-column retrieval uncertainty, cloud and surface effects, and spatial representativeness.

## 1 Introduction

Nitrogen dioxide ($NO_2$) is an important reactive nitrogen species in the troposphere and is closely linked to air quality, atmospheric oxidation capacity, and climate-relevant chemical processes. It is mainly produced as part of nitrogen oxides ($NO_x = NO + NO_2$) emitted from fossil fuel combustion, road traffic, power generation, industrial activities, and biomass burning. Through photochemical reactions, $NO_2$ contributes to the formation of tropospheric ozone ($O_3$) and nitrate aerosols, thereby affecting both human health and atmospheric composition (Monks et al., 2015; Krotkov et al., 2016). Because its lifetime is relatively short, the spatial and temporal variability of $NO_2$ reflects the distribution of emission sources as well as boundary-layer mixing, transport, and chemical loss processes. Satellite observations are therefore essential for monitoring $NO_2$ over broad regions, especially where ground-based air-quality networks are sparse or unevenly distributed (Krotkov et al., 2016; Veefkind et al., 2012).

Spaceborne ultraviolet–visible (UV–Vis) spectroscopy has played a major role in the development of tropospheric $NO_2$ observation technology, from earlier low-Earth-orbit (LEO) sensors such as the Global Ozone Monitoring Experiment (GOME), GOME-2, the Scanning Imaging Absorption Spectrometer for Atmospheric Chartography, the Ozone Monitoring Instrument (OMI), and the Ozone Mapping and Profiler Suite, to the more recent TROPOspheric Monitoring Instrument (TROPOMI) aboard the Sentinel-5 Precursor (S5P) satellite (Veefkind et al., 2012; van Geffen et al., 2022). With its improved spatial resolution and radiometric performance, TROPOMI has made it possible to resolve much finer-scale $NO_2$ structures than was previously feasible from LEO platforms, including enhancements associated with urban areas, industrial facilities, harbours, and airports (Veefkind et al., 2012; Griffin et al., 2019). At the same time, satellite air-quality monitoring is entering a new phase with the emergence of geostationary Earth orbit (GEO) missions, including the Geostationary Environment Monitoring Spectrometer over East Asia, Tropospheric Emissions: Monitoring of Pollution over North America, and the

https://doi.org/10.5194/egusphere-2026-4968
Preprint. Discussion started: 11 September 2026


Sentinel-4 Ultraviolet Visible Near-infrared Spectrometer over Europe (Kim et al., 2020; Zoogman et al., 2017; Ingmann et al., 2012). By providing observations at much higher temporal frequency, these GEO instruments are expected to complement polar-orbiting sensors and provide new constraints on the diurnal evolution of $NO_2$, emission timing, species transport, and photochemical processing (Kim et al., 2020; Zoogman et al., 2017). Despite these advances, satellite retrievals of tropospheric $NO_2$ data remain strongly dependent on the assumptions used to convert the measured slant column density (SCD) into a vertical column density (VCD). This conversion is performed using an air mass factor (AMF), which represents the sensitivity of the satellite measurement to $NO_2$ distributed within the atmosphere (Boersma et al., 2018; van Geffen et al., 2022). The AMF is not a fixed quantity; rather, it varies with viewing geometry, surface reflectance, cloud and aerosol conditions, terrain height, atmospheric scattering, and the assumed vertical distribution of $NO_2$ (Lorente et al., 2017). Among these factors, the a priori $NO_2$ profile is particularly important over polluted regions, where a large fraction of the $NO_2$ column is often confined to the lower troposphere. If this near-surface enhancement is misplaced or underestimated in the a priori profile, the AMF can be biased, leading directly to systematic errors in the retrieved tropospheric $NO_2$ VCD (Lorente et al., 2017; van Geffen et al., 2022; Riess et al., 2023).

Substantial effort has therefore been devoted to reducing AMF-related uncertainties in satellite $NO_2$ retrievals. Earlier developments focused on improving the key inputs to the retrieval framework, including chemical transport model-based a priori $NO_2$ profiles, surface reflectance information, cloud treatment, and the separation of stratospheric and tropospheric columns (Boersma et al., 2018; van Geffen et al., 2022). For example, the Quality Assurance for Essential Climate Variables project provided improved $NO_2$ retrieval algorithms and uncertainty estimates for OMI and GOME-2 observations (Boersma et al., 2018). Lorente et al. (2017) further showed that structural uncertainties in AMF calculations are a major source of error in satellite retrievals of both $NO_2$ and formaldehyde (HCHO) data. For TROPOMI, algorithm updates in the version 2 product introduced improvements related to cloud pressure, surface albedo climatology, TM5-MP model a priori profiles, and snow/ice treatment, which helped reduce the negative biases previously reported over polluted regions (van Geffen et al., 2022).

Another important direction has been to represent aerosol, surface, and cloud effects more explicitly in the AMF calculation. Using the Peking University OMI $NO_2$ product (POMINO), Lin et al. (2014, 2015) examined how aerosol scattering and absorption, surface reflectance anisotropy, and the assumed vertical distribution of $NO_2$ affect OMI $NO_2$ retrievals. Their results showed that these factors can substantially modify the retrieved $NO_2$ columns, particularly over highly polluted regions such as China and East Asia. Building on this line of work, Liu et al. (2019) improved the aerosol correction for OMI $NO_2$ retrievals over East Asia by constraining aerosol vertical distributions with Cloud-Aerosol Lidar with Orthogonal Polarization observations. Liu et al. (2020) then extended this approach to TROPOMI by developing a POMINO-TROPOMI $NO_2$ product with explicit aerosol corrections. In a separate regional research product over Europe, Liu et al. (2021) combined updates to surface albedo, a priori $NO_2$ profiles, and cloud treatment to improve TROPOMI tropospheric $NO_2$ columns. Together, these studies demonstrate that $NO_2$ retrieval errors cannot be attributed to a single retrieval parameter alone, but arise from the combined radiative effects of the surface, aerosols, clouds, viewing geometry, and vertical position of $NO_2$ in the atmosphere (Lorente et al., 2017; Liu et al., 2020; Liu et al., 2021).

Clouds introduce another important source of uncertainty in satellite $NO_2$ retrievals. Depending on their altitude, optical thickness, cloud fraction, and cloud radiance fraction within a satellite pixel, clouds can either shield $NO_2$ located below the cloud layer or enhance the light path through multiple scattering, thereby altering the AMF and the retrieved tropospheric $NO_2$ VCD (Latsch et al., 2022; van Geffen et al., 2022). Intercomparisons of cloud products used in TROPOMI trace-gas retrievals have shown that differences in cloud fraction, cloud pressure, and related cloud parameters can lead to systematic differences in UV–Vis trace-gas columns (Latsch et al., 2022). The problem is particularly challenging for partly cloudy scenes, where the spatial distribution of $NO_2$ within the pixel may not be consistent with the simplified cloud representation used in the retrieval. Lim et al. (2026) recently demonstrated, using a TROPOMI-based assessment for Thermal and Near-infrared Sensor for Carbon Observation-3 aboard the Global Observing Satellite for Greenhouse Gases and Water Cycle $NO_2$ processing, that accounting for scattering clouds can improve $NO_2$ AMF calculations. Their results highlight that clouds should not be treated only as obscuring features, but also as radiative elements that modify photon pathways and measurement sensitivity. These findings indicate that, in addition to strict clear-sky filtering, more realistic treatment of cloud representativeness and sub-pixel heterogeneity is important for further reducing AMF-related uncertainties (Latsch et al., 2022; Lim et al., 2026).

Independent ground-based validation is essential for assessing the reliability of satellite $NO_2$ observation products. Such comparisons, however, are not straightforward because satellite $NO_2$ VCDs represent averages over finite pixel areas, whereas ground-based instruments are sensitive to a fixed location or to a specific viewing direction and light path (Verhoelst et al., 2021; Judd et al., 2020). This scale mismatch introduces unavoidable uncertainties in spatiotemporal representativeness, especially in regions where $NO_2$ varies sharply over short distances. Despite these challenges, ground-based remote-sensing networks have provided critical reference data for evaluating satellite $NO_2$ retrievals. Measurements from Multi-Axis Differential Optical Absorption Spectroscopy (MAX-DOAS), Pandora direct-sun spectrometers, and the Network for the Detection of Atmospheric Composition Change (NDACC) zenith-sky DOAS (ZSL-DOAS) network have been widely used to quantify biases, random errors, seasonal variability, and pollution-regime dependence in satellite-acquired $NO_2$ columns (Herman et al., 2009; Verhoelst et al., 2021). Herman et al. (2009) demonstrated the use of Pandora direct-sun $NO_2$ columns for validating OMI observations, while Verhoelst et al. (2021) provided a global validation of TROPOMI $NO_2$ data using NDACC ZSL-DOAS, MAX-DOAS, and Pandora observations. These studies showed that TROPOMI generally captures the temporal variability of tropospheric $NO_2$, but it can exhibit systematic low biases under polluted conditions, pointing to remaining uncertainties in AMF calculations and observation representativeness (Verhoelst et al., 2021; van Geffen et al., 2022).

MAX-DOAS observations are particularly useful in this context because they can provide information on the vertical distribution of $NO_2$ in the lower troposphere, in addition to column amounts. This capability allows ground-based measurements to be used not only for satellite validation, but also for diagnosing errors in the AMF calculation itself. Dimitropoulou et al. (2020) validated TROPOMI tropospheric $NO_2$ columns over Brussels using dual-scan MAX-DOAS measurements and showed that recalculating the TROPOMI AMF with MAX-DOAS-derived $NO_2$ profiles can lead to substantially larger satellite $NO_2$ columns. Chan et al. (2020) also compared OMI and TROPOMI $NO_2$ observations with

https://doi.org/10.5194/egusphere-2026-4968
Preprint. Discussion started: 11 September 2026


MAX-DOAS measurements in Munich and emphasized the importance of ground-based profile information for interpreting satellite retrieval biases. These studies indicate that one of the key limitations in satellite $NO_2$ retrievals is not simply the comparison of column amounts, but the extent to which the retrieval represents the actual near-surface $NO_2$ vertical distribution (Dimitropoulou et al., 2020; Chan et al., 2020; Riess et al., 2023).

Beyond the vertical profile issue, horizontal representativeness remains a major challenge in ground-based validation of satellite $NO_2$ products. MAX-DOAS and Pandora sky-scan observations are not necessarily sensitive only to the air directly above the instrument; depending on the viewing geometry and atmospheric conditions, their effective sampling paths can extend over several to tens of kilometres. Even direct-sun Pandora measurements contain information integrated along the solar light path rather than from an idealized point column. As a result, a simple radius-based collocation between satellite pixels and a ground site may not fully capture the air mass to which the ground-based observation is most sensitive. Chi et al. (2025) recently characterized Pandora sky-scan modes within the Japan Pandora Network and evaluated the horizontal light path length, showing that the spatial representativeness of Pandora observations needs to be considered more explicitly when they are used to validate satellite $NO_2$ and HCHO observations. This issue is especially relevant over spatially heterogeneous environments such as urban areas, coastal regions, and airports, where wind direction, source location, viewing geometry, and the satellite pixel footprint can all influence the interpretation of satellite–ground comparisons (Judd et al., 2020; Chi et al., 2025).

To better constrain the vertical distribution of $NO_2$, aircraft measurements have also been used as an independent source of information for satellite retrieval evaluation. Unlike satellite retrievals or most ground-based remote-sensing observations, aircraft can sample $NO_2$ directly within the atmosphere and can provide vertical profile information, including in the lower troposphere, where the AMF is particularly sensitive to the assumed $NO_2$ distribution. Aircraft in situ measurements and airborne imaging DOAS observations have been used to evaluate TROPOMI tropospheric $NO_2$ VCDs and to investigate sub-pixel spatial variability that is difficult to resolve from space (Griffin et al., 2019; Judd et al., 2020; Tack et al., 2021; Lange et al., 2023). Riess et al. (2023) more directly connected aircraft profile measurements to the AMF problem by comparing aircraft-observed vertical $NO_2$ profiles with model simulations used in TROPOMI retrievals. They showed that replacing the TM5-MP a priori profile with aircraft-based profiles can lead to appreciable changes in the retrieved $NO_2$ columns. This finding illustrates the value of observed vertical profile information for diagnosing AMF-related retrieval errors and for interpreting satellite $NO_2$ biases over polluted lower-tropospheric environments (Riess et al., 2023).

The In-service Aircraft for a Global Observing System (IAGOS) provides long-term, routine measurements of atmospheric composition using instruments installed on commercial passenger aircraft (Petzold et al., 2015). Although IAGOS observations are widely used to investigate atmospheric composition in the upper troposphere and lowermost stratosphere along cruise flight tracks, the ascent and descent portions of these flights also provide vertical profiles near airports (Petzold et al., 2015; Berkes et al., 2018). These lower-tropospheric profiles are well suited for examining TROPOMI $NO_2$ AMF sensitivity because the retrieval is strongly affected by the vertical position of $NO_2$ near the surface. Berkes et al. (2018) described the design and operation of the IAGOS $NO_x$ instrument and demonstrated its capability for routine $NO_x$ measurements from commercial aircraft. IAGOS profiles therefore provide an observational basis for testing how aircraft-derived lower-tropospheric $NO_2$ information affects TROPOMI AMFs, particularly over airport environments where independent Pandora observations are available nearby.

In this study, we combined IAGOS airborne measurements, TROPOMI tropospheric $NO_2$ VCDs, and Pandora observations near airports to investigate how lower-tropospheric $NO_2$ profile variability affects satellite-derived tropospheric $NO_2$ columns. The analysis focused on airport–Pandora pairs in Japan, South Korea, and Thailand during March–July 2025, when coincident TROPOMI observations and IAGOS descent profiles are available. We first examined whether the temporal variability of TROPOMI $NO_2$ around the selected Pandora sites is representative of that around the corresponding airports. This step provided a basis for interpreting Pandora-based validation results in airport environments, where $NO_2$ fields can be spatially heterogeneous. We then used lower-tropospheric $NO_2$ profile information derived from IAGOS observations to recalculate TROPOMI AMFs and evaluate both the operational and IAGOS-profile-recalculated TROPOMI $NO_2$ VCDs against nearby Pandora measurements. Through this approach, we quantified the sensitivity of TROPOMI $NO_2$ retrievals to lower-tropospheric profile assumptions near airports and assessed whether IAGOS profiles can provide a complementary observational constraint linking satellite column retrievals with ground-based validation.

The remainder of this paper is organized as follows. Section 2 describes the study domain and the observational datasets, namely those obtained by TROPOMI, Pandora, and IAGOS, as well as the TM5-MP a priori profiles. Section 3 presents the collocation procedure, the construction of observation-constrained $NO_2$ profiles, and the AMF and VCD recalculation method. Section 4 evaluates the airport–Pandora representativeness, compares the TM5-MP and observation-constrained $NO_2$ profiles, and assesses the impacts of the profile changes on TROPOMI AMFs and VCDs. Section 5 discusses the remaining Pandora-scaled residuals from a spatial-heterogeneity and SCD-equivalent closure perspective. Section 6 summarises the main findings and implications for using aircraft and ground-based profile information to improve satellite $NO_2$ retrievals near airports.

## 2 Data and study domain

This section describes the observational and auxiliary datasets used to evaluate the influence of lower-tropospheric $NO_2$ profile information on TROPOMI AMF calculations near airports. The analysis combined satellite $NO_2$ retrievals from TROPOMI, ground-based Pandora observations, and aircraft in situ profiles from IAGOS. The study focused on selected airport–Pandora pairs in East and Southeast Asia, where IAGOS descent profiles are available near major airports and Pandora observations are available within the surrounding region. TM5-MP a priori profiles used in the operational TROPOMI $NO_2$ retrieval were also used as a reference for the AMF recalculation.

https://doi.org/10.5194/egusphere-2026-4968
Preprint. Discussion started: 11 September 2026


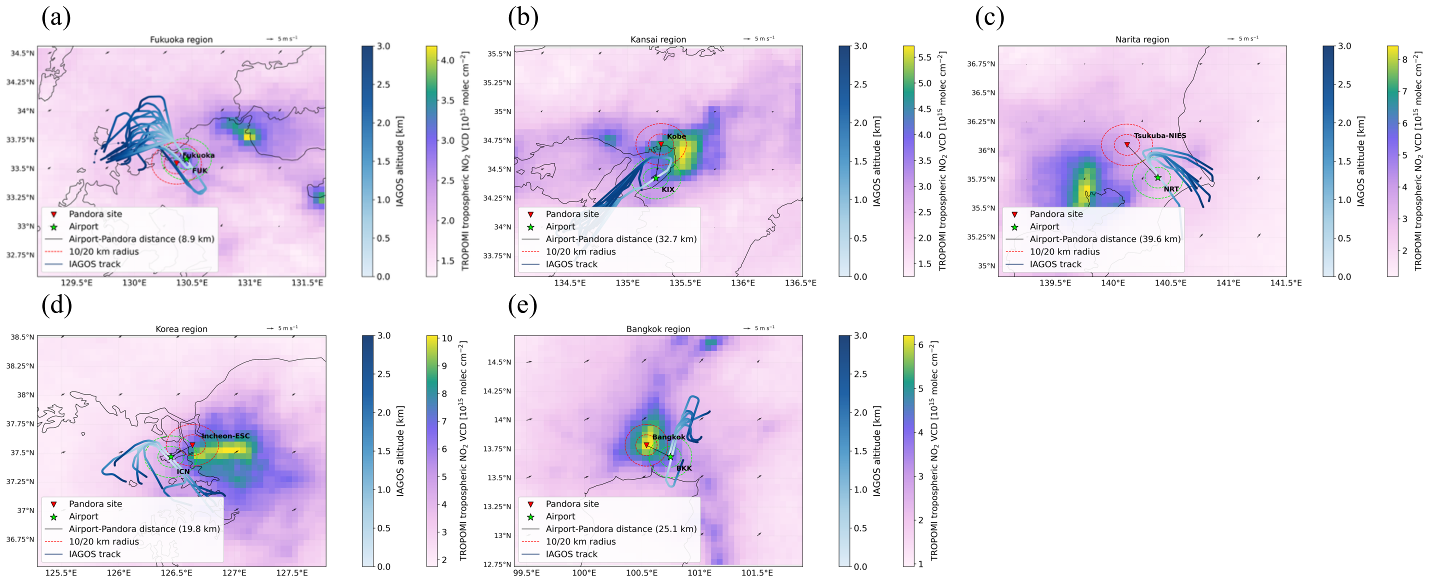


Figure 1. Study regions and airport–Pandora pairs used in this study. The background shows the regridded mean TROPOMI tropospheric $NO_2$ VCD from March to July 2025. Stars and inverted triangles indicate the airport locations and Pandora sites, respectively. The circles represent the spatial averaging radii used to calculate $NO_2$ VCDs around each airport and Pandora site. IAGOS descent tracks near each airport are overlaid and coloured by altitude.

## 2.1 Study region and airport–Pandora pairs

The study domain included five airport–Pandora pairs located in Japan, South Korea, and Thailand. These pairs were selected based on the availability of IAGOS descent profiles near airports during March–July 2025 and the presence of nearby Pandora $NO_2$ observations that can be used for independent evaluation of the satellite retrievals. The selected airport are Fukuoka (FUK), Kansai (KIX), Narita (NRT), Incheon (ICN), and Bangkok (BKK). The corresponding Pandora sites are Fukuoka, Kobe, Tsukuba-NIES, Incheon-ESC, and Bangkok, respectively. Figure 1 shows the spatial distribution of the selected airports and Pandora sites, together with the regridded mean TROPOMI tropospheric $NO_2$ VCD during March–July 2025. The figure illustrates the contrasting spatial environments of the selected pairs, including relatively short airport–Pandora separations, such as FUK–Fukuoka, and longer separations, such as NRT–Tsukuba-NIES. These differences are important because the spatial representativeness of Pandora observations can affect the interpretation of satellite validation results, particularly in regions where $NO_2$ fields show strong horizontal gradients around emission sources such as urban areas, coastal zones, and airports.

The geographic coordinates of the airports and Pandora sites, together with the airport–Pandora distances, are given in Table 1. The airport–Pandora distances range from 8.9 km for FUK–Fukuoka to 39.6 km for NRT–Tsukuba-NIES. This range allows us to examine how the spatial separation between the airport and the ground-based reference site influences the consistency between airport-scale and Pandora-site $NO_2$ variability.

https://doi.org/10.5194/egusphere-2026-4968
Preprint. Discussion started: 11 September 2026


### 2.2 TROPOMI $NO_2$ product and TM5-MP a priori profiles

We used the S5P TROPOMI $NO_2$ Level-2 product version 2.8.0 for the period from March to July 2025 (van Geffen et al., 2024). The product provides tropospheric $NO_2$ VCDs retrieved from UV–Vis backscattered solar radiation, along with diagnostic quantities such as the tropospheric AMF, averaging kernel (AK), and quality assurance (QA) values. For the analysis, we retained only pixels with a QA value ≥ 0.75. This screening was applied to limit the influence of retrievals affected by clouds, snow or ice, large fitting uncertainties, and other conditions that may reduce the reliability of the $NO_2$ product. The selected TROPOMI pixels were used to characterize $NO_2$ around each airport and Pandora site and to support the subsequent AMF recalculation and Pandora-based evaluation. In the operational TROPOMI $NO_2$ retrieval, the tropospheric AMF depends on the a priori vertical $NO_2$ profile provided by the TM5-MP chemistry transport model (Williams et al., 2017).

Table 1. Locations of the selected airports and Pandora sites used in this study. The distance indicates the horizontal separation between each airport and its corresponding Pandora site.

| Country | Airport | Airport location (lon., lat.) | Pandora site (instrument ID) | Pandora location (lon., lat.) | Distance [km] |
|---|---|---|---|---|---|
| Japan | Fukuoka (FUK) | 130.451, 33.586 | Fukuoka (Pandora199s1) | 130.380, 33.590 | 6.6 |
| | Kansai (KIX) | 135.244, 34.427 | Kobe (Pandora198s1) | 135.190, 34.690 | 29.7 |
| | Narita (NRT) | 140.388, 35.768 | Tsukuba-NIES (Pandora176s1) | 140.121, 36.050 | 39.5 |
| South Korea | Incheon (ICN) | 126.451, 37.469 | Incheon-ESC (Pandora189s1) | 126.640, 37.560 | 19.5 |
| Thailand | Bangkok (BKK) | 100.748, 13.685 | Bangkok (Pandora190s1) | 100.565, 13.760 | 21.5 |

### 2.3 Pandora observations

We used Pandora observations from the Pandonia Global Network to provide ground-based $NO_2$ profile information near the selected airports. The Pandora sites used in this study were Fukuoka, Kobe, Tsukuba-NIES, Incheon-ESC, and Bangkok, which were paired with FUK, KIX, NRT, ICN, and BKK, respectively. The locations of the Pandora instruments, their instrument IDs, and the distances from the corresponding airports are summarised in Table 1. Pandora instruments can operate in both direct-sun and sky-scan modes in the UV–Vis spectral range (Mouat et al., 2024; Rawat et al., 2025). Direct-sun measurements observe the solar beam directly and provide $NO_2$ column information integrated along the solar light path; this observing mode

https://doi.org/10.5194/egusphere-2026-4968
Preprint. Discussion started: 11 September 2026


has been widely used for satellite $NO_2$ column validation. In contrast, sky-scan measurements collect scattered sunlight at multiple viewing directions, providing information on the lower-tropospheric $NO_2$ vertical distribution and the spatial sensitivity of the observation. Sky-scan observations therefore help us examine lower-tropospheric profile characteristics that are important for satellite $NO_2$ retrievals. In this study, Pandora sky-scan $NO_2$ profile information was used to characterize lower-tropospheric $NO_2$ vertical distributions near the selected airports and to provide ground-based constraints for the AMF recalculation.

### 2.4 IAGOS $NO_2$ airborne data

In this study, aircraft-based observations of lower-tropospheric $NO_2$ vertical distributions around airports were taken from the $NO_2$ mixing ratio profiles provided by the IAGOS-CORE Package 2b (P2b) $NO_x$ instrument. IAGOS is a research infrastructure that provides long-term atmospheric composition measurements using automated in situ instruments installed on commercial aircraft (Petzold et al., 2015). The P2b instrument was developed for automated measurements of $NO_x$ (NO + $NO_2$). It detects chemiluminescence from the reaction between ambient NO and $O_3$. $NO_2$ is first converted to NO by a UV LED photolytic converter, and NO and $NO_x$ are then measured sequentially by switching the converter LED on and off (Berkes et al., 2018). In this work, we used the $NO_2$ mixing ratio reported as a separate variable in the IAGOS Level 2 product.

IAGOS profiles observed from March to July 2025 near the selected airports in Japan, South Korea, and Thailand were used in the analysis. Only descent profiles were included in the AMF recalculation because ascent profiles only receive non-validated QA/QC flags in the IAGOS $NO_x$ data stream. This considers the detector cooldown phase after instrument startup and the possibility of ground contamination. The IAGOS $NO_2$ data from near the surface to approximately 3 km were then used to constrain the lower-tropospheric part of the a priori profile, where the TROPOMI $NO_2$ AMF is most sensitive to the vertical distribution of $NO_2$.

The IAGOS $NO_2$ profiles were regridded to the same vertical layer structure as that of the TM5-MP a priori profiles used in the TROPOMI operational retrieval, enabling a direct comparison between the aircraft- and model-based $NO_2$ vertical distributions.

## 3 Method

### 3.1 Collocation of TROPOMI, Pandora, and IAGOS observations

For each airport–Pandora pair, TROPOMI observations were collocated using the same spatial sampling procedure around the airport and the corresponding Pandora site. For every TROPOMI overpass, a circular sampling area with a radius of 10 km was defined around each location, and all valid TROPOMI pixels falling within the circle were extracted. The quality filtering described in Sect. 2.2 was applied before any spatial averaging was performed. For each overpass, tropospheric $NO_2$ VCDs were averaged separately over the airport-centred and Pandora-centred sampling areas. The airport-centred average was used to represent the satellite-observed $NO_2$ condition near the IAGOS flight profile, whereas the Pandora-centred average represented the satellite $NO_2$ condition around the ground-based site. Because the same sampling radius and quality criteria were applied to both locations, the resulting time series provided a consistent basis for comparing $NO_2$ variability between the airport and Pandora regions. These paired time series were later used to examine how well the Pandora observations represent temporal variations in $NO_2$ around the airport. IAGOS descent profiles were matched to TROPOMI overpasses based on their location and observation time. The representative time of each IAGOS profile was defined as the median observation time within the 0–3 km altitude range used for the AMF recalculation. When this median time was within 1 h of the TROPOMI overpass time, the IAGOS profile was used without any temporal adjustment. When the time difference was larger than 1 h, a temporal correction was applied using the diurnal variation of $NO_2$ observed by Pandora. This correction adjusted the overall magnitude of the IAGOS $NO_2$ profile to the TROPOMI overpass time, while keeping the vertical shape measured by the aircraft unchanged.

### 3.2 Construction of observation-scaled $NO_2$ vertical profiles

To recalculate the TROPOMI $NO_2$ AMF, the operational TM5-MP a priori profile and the observation-based $NO_2$ profiles must be represented on a common vertical grid. We therefore mapped the $NO_2$ profile information from IAGOS and Pandora onto the TM5-MP vertical layer structure used in the operational TROPOMI retrieval. For the IAGOS profiles, $NO_2$ mixing ratios were averaged within each TM5-MP layer to obtain layer-specific mean mixing ratios. When more than one IAGOS measurement was available within a given layer, the arithmetic mean was used. Negative $NO_2$ mixing ratios, when present, were set to zero before layer averaging. The layer mean mixing ratios were then converted to partial $NO_2$ columns using the pressure thickness of each layer. The IAGOS-scaled profile was constructed by replacing the lower part of the TM5-MP a priori profile with the IAGOS-derived partial $NO_2$ columns. In this study, the replacement was applied from the lowest available altitude to approximately 3 km, where the aircraft observations directly constrain the lower-tropospheric $NO_2$ distribution around the airport. Above 3 km, the original TM5-MP a priori profile was retained. This approach maintained the model-based profile structure in the free troposphere, while allowing the lower-tropospheric part of the profile, which is particularly important for the AMF calculation, to reflect the aircraft observations.

Pandora-derived $NO_2$ profiles were processed in the same TM5-MP layer framework. These profiles provide a ground-based constraint on the lower-tropospheric $NO_2$ distribution and were used as the Pandora-scaled profile case for comparison with the IAGOS-scaled and TM5-MP profiles. When temporal correction of the IAGOS profile was required, the correction described in Sect. 3.1 was applied before mapping the profile onto the TM5-MP layers.

Three profile cases were prepared for the AMF recalculation. The first case used the original TM5-MP a priori profile from the operational retrieval. The second case used the IAGOS-scaled profile, in which the lower-tropospheric part of the TM5-MP profile was replaced by the IAGOS-scaled profile. When required, the IAGOS profile was first temporally adjusted using

https://doi.org/10.5194/egusphere-2026-4968
Preprint. Discussion started: 11 September 2026


the Pandora $NO_2$ diurnal variation. The third case used the Pandora-scaled profile as a ground-based observation-scaled profile. These three profile cases were then used as input profiles for the AMF recalculation described in Sect. 3.3.

### 3.3 Recalculation of tropospheric $NO_2$ AMF and VCD

To quantify the effect of the observation-scaled $NO_2$ vertical profiles described in Sect. 3.2, we recalculated the TROPOMI tropospheric $NO_2$ AMF using the operational tropospheric AMF and AK provided in the product. In this recalculation, the viewing geometry, cloud parameters, surface reflectance, and radiative transfer conditions for each TROPOMI pixel were kept the same as in the operational retrieval. Therefore, any change in the AMF was attributed only to the change in the a priori $NO_2$ vertical profile. The tropospheric $NO_2$ AMF can be written as a partial-column-weighted mean of the layer scattering weights:

$$M = \frac{\Sigma m_l x_l}{\Sigma x_l}, \tag{1}$$

where $M$ is the tropospheric AMF, $m_l$ is the scattering weight for layer $l$, and $x_l$ is the $NO_2$ partial column in that layer (Palmer et al., 2001; Eskes and Boersma, 2003). In the operational retrieval, $x_l$ was determined from the TM5-MP a priori profile. In this study, the layer-dependent scattering weights were reconstructed from the operational AMF and AK provided in the TROPOMI product. The original $x_l$ was then replaced by the observation-scaled $NO_2$ partial columns defined in Sect. 3.2. The recalculated AMF was obtained as

$$M_{new} = \frac{\Sigma m_l x_{l,new}}{\Sigma x_{l,new}}, \tag{2}$$

where $x_{l,new}$ denotes the partial $NO_2$ column constrained by the IAGOS or Pandora profile. The scattering weights $m_l$ were kept unchanged from those for the operational retrieval. No new radiative transfer calculation was performed; only the $NO_2$ vertical profile was changed while the layer sensitivity was kept fixed. After recalculating the AMF, the tropospheric $NO_2$ VCD was updated by assuming that the retrieved SCD remained unchanged. The relationship between the operational VCD and AMF was used to calculate the updated tropospheric $NO_2$ VCD as

$$VCD_{new} = VCD_{operational} \times \left(\frac{M_{operational}}{M_{new}}\right). \tag{3}$$

With this formulation, a smaller recalculated AMF gives a larger VCD, and a larger recalculated AMF gives a smaller VCD. This relationship was used to quantify the differences in AMF and VCD between the operational case based on the TM5-MP a priori profile and the cases using IAGOS- or Pandora-scaled profiles. The AMF and VCD recalculations were first performed at the individual TROPOMI pixel level. The recalculated pixel-level values were then averaged within the 10 km airport- and Pandora-centred sampling areas defined in Sect. 3.1 to obtain representative values for each overpass. The resulting operational and recalculated tropospheric $NO_2$ VCDs were used for the Pandora comparison and statistical evaluation described in Sect.4.

https://doi.org/10.5194/egusphere-2026-4968
Preprint. Discussion started: 11 September 2026


The operational and recalculated TROPOMI tropospheric $NO_2$ VCDs were evaluated against Pandora observations using the same matched samples for each airport–Pandora pair. The comparison was summarised using the number of matched samples (N), Pearson correlation coefficient (R), mean bias error (MBE), root-mean-square error (RMSE), and the fraction of data points satisfying the Global Climate Observing System (GCOS) goal criterion. The MBE was calculated as the mean difference between TROPOMI and Pandora $NO_2$ VCDs, and the RMSE was used to describe the overall magnitude of the differences. A matched data point was counted as satisfying the GCOS goal criterion when the absolute difference between TROPOMI and Pandora was smaller than max (20 % of the Pandora $NO_2$ VCD, $1 \times 10^{15}$ molec cm$^{-2}$), following the GCOS requirement for tropospheric $NO_2$ column measurements (GCOS, 2026). These statistics were used to compare the operational and recalculated VCDs on a common basis.

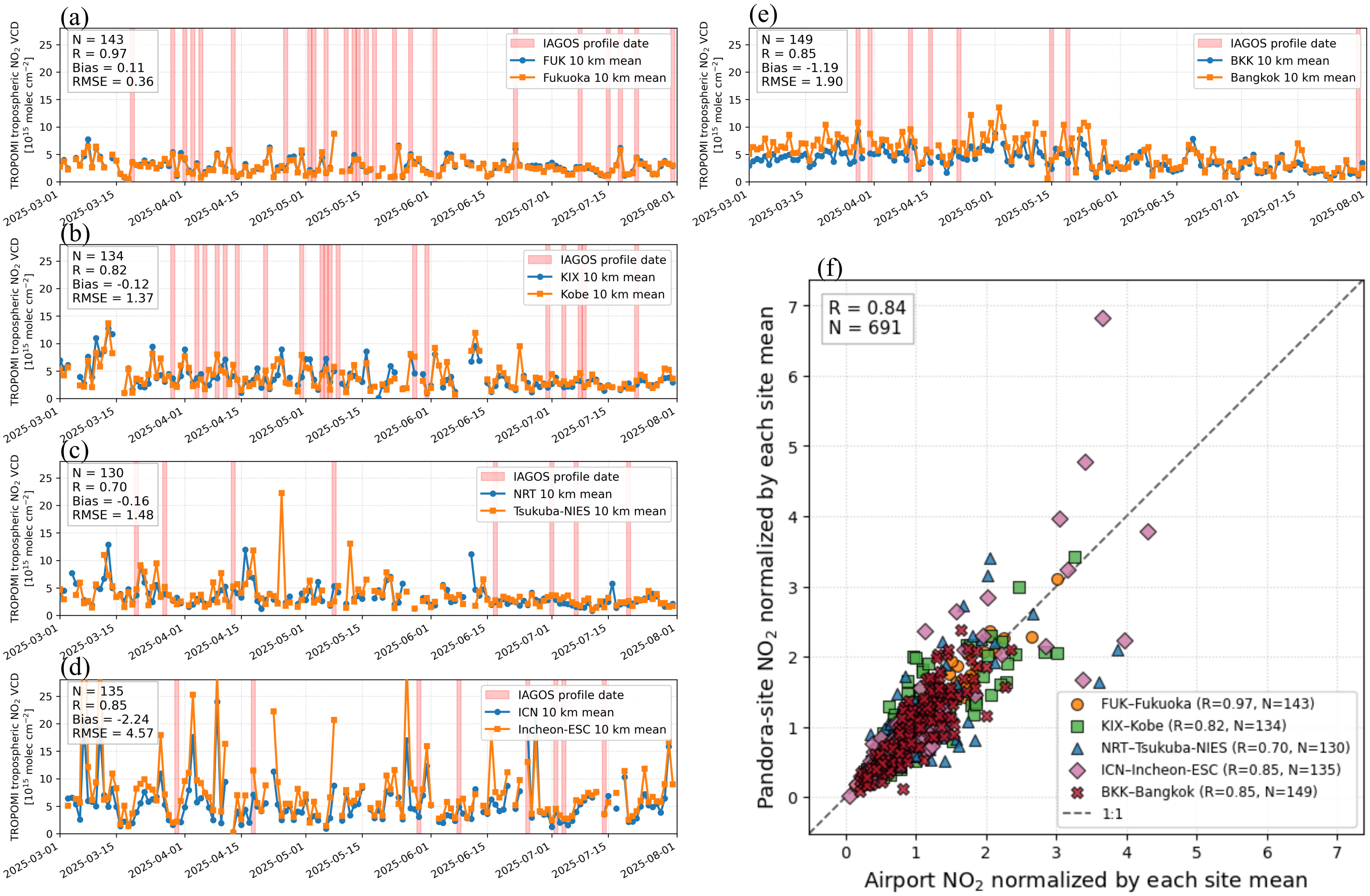


Figure 2. Temporal variation of TROPOMI tropospheric $NO_2$ VCDs around each airport and its corresponding Pandora site. Panels (a)–(e) show the 10 km mean TROPOMI $NO_2$ VCD time series for FUK, KIX, NRT, ICN, and BKK, respectively. Blue and orange lines indicate the airport-centered and Pandora-site-centered TROPOMI $NO_2$ VCDs, respectively. Red shading indicates dates with available IAGOS descent profiles. Panel (f) compares the airport-region and Pandora-region $NO_2$ VCDs after normalization by each site mean.

https://doi.org/10.5194/egusphere-2026-4968
Preprint. Discussion started: 11 September 2026


## 4 Results

This section examines the role of observation-scaled $NO_2$ vertical profiles in the TROPOMI tropospheric $NO_2$ AMF and VCD calculations. We begin by comparing the temporal variability of the satellite $NO_2$ fields around the airports with that around the corresponding Pandora sites. This comparison is needed because the Pandora instruments were located away from the airports, and the two sites may differ in their absolute $NO_2$ levels. We next examine how the lower-tropospheric $NO_2$ profiles derived from IAGOS and Pandora differ from the TM5-MP a priori profiles used in the operational retrieval. These profile differences are then linked to changes in the recalculated AMFs. Finally, the operational and recalculated TROPOMI tropospheric $NO_2$ VCDs are evaluated against Pandora observations to assess how the observation-scaled profiles affect the agreement with the ground-based reference data.

### 4.1 Temporal consistency and spatial representativeness of airport- and Pandora-region $NO_2$

Before comparing the profile-based AMF recalculation results with Pandora observations, we first examined whether the satellite $NO_2$ field around each airport varied consistently with that around the corresponding Pandora site. The airport and Pandora sites are not located at the same position, and for some airport–Pandora pairs, the separation reaches several tens of kilometres. The absolute TROPOMI $NO_2$ VCD levels can therefore differ between the two regions. If the two sets of satellite $NO_2$ time series show similar temporal variability, however, the satellite $NO_2$ field around the Pandora site can help provide a context for interpreting $NO_2$ variability around the airport. Figures 2(a)–(e) show the TROPOMI tropospheric $NO_2$ VCD time series averaged within 10 km of each airport and its corresponding Pandora site. Red shading indicates the dates on which IAGOS descent profiles were available, allowing the satellite $NO_2$ conditions at the time of aircraft profile observations to be identified. Figure 2(f) compares the airport- and Pandora-region TROPOMI $NO_2$ time series after normalizing each time series by its own mean. Here, the Pandora-region $NO_2$ does not refer to the Pandora retrieval itself, but to the TROPOMI $NO_2$ VCD sampled around the Pandora site. The normalization of the TROPOMI $NO_2$ removes differences in the mean $NO_2$ level between the two regions and emphasizes their relative temporal variability. The normalized $NO_2$ VCDs show a clear positive relationship across the matched dataset, indicating that increases in satellite-observed $NO_2$ around the airport generally coincided with increases observed by the Pandora site. This result does not imply that the airport and Pandora regions have the same absolute $NO_2$ level. Mean $NO_2$ conditions and local emission influences can differ from site to site. Nevertheless, the co-variation between the airport-region and Pandora-region TROPOMI $NO_2$ time series provides useful information on the spatial representativeness of the Pandora-site region, which is needed when interpreting the subsequent Pandora-based evaluation of satellite $NO_2$.

Figure 3 summarises the temporal consistency and mean difference between the airport- and Pandora-region TROPOMI $NO_2$ VCDs for each airport–Pandora pair. The y-axis gives the temporal correlation coefficient between the two regional time series, and the x-axis gives the mean bias, defined as the airport-region mean minus the Pandora-region mean. Colour indicates the

https://doi.org/10.5194/egusphere-2026-4968
Preprint. Discussion started: 11 September 2026


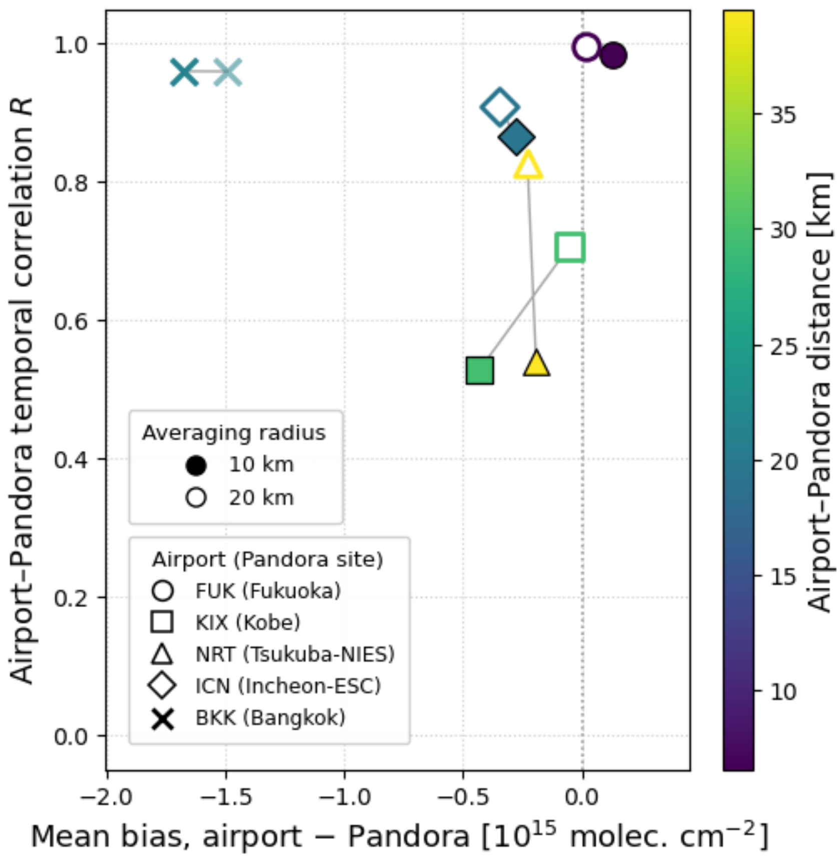


Figure 3. Summary of the representativeness between airport-region and Pandora-region TROPOMI $NO_2$ VCDs. The y-axis indicates the temporal correlation coefficient between the two regional time series, and the x-axis indicates the mean bias, defined as the airport-region minus the Pandora-region $NO_2$ VCD.

distance between the airport and the Pandora site, while filled and open symbols denote results based on 10 km and 20 km averaging radii, respectively. All airport–Pandora pairs showed positive temporal correlations, suggesting that the two regional satellite $NO_2$ time series generally captured similar temporal variability. The mean bias, however, differed among sites. FUK–Fukuoka showed both a high temporal correlation and a small mean difference, consistent with the short distance between the airport and the Pandora site. BKK–Bangkok, in contrast, showed a clear negative mean bias despite its high temporal correlation, indicating that the Pandora-region $NO_2$ level was systematically higher than that around the airport, while the temporal variation remained similar. KIX–Kobe and NRT–Tsukuba-NIES showed relatively larger sensitivity to the averaging radius, suggesting that the choice of spatial averaging scale can affect the estimated representativeness between the airport and Pandora regions. The Pandora region does not always reproduce the absolute $NO_2$ level around each airport. Such differences can become more important when the two locations are separated by several tens of kilometres or are influenced by different local emission environments. At the same time, the generally positive temporal correlations indicate that the satellite $NO_2$ field

https://doi.org/10.5194/egusphere-2026-4968
Preprint. Discussion started: 11 September 2026


380 around the Pandora site provides information for interpreting temporal changes in satellite $NO_2$ around the airport. Distinguishing temporal consistency from absolute spatial bias is therefore important for the Pandora-based evaluation of the recalculated TROPOMI $NO_2$ VCDs discussed in the following sections.

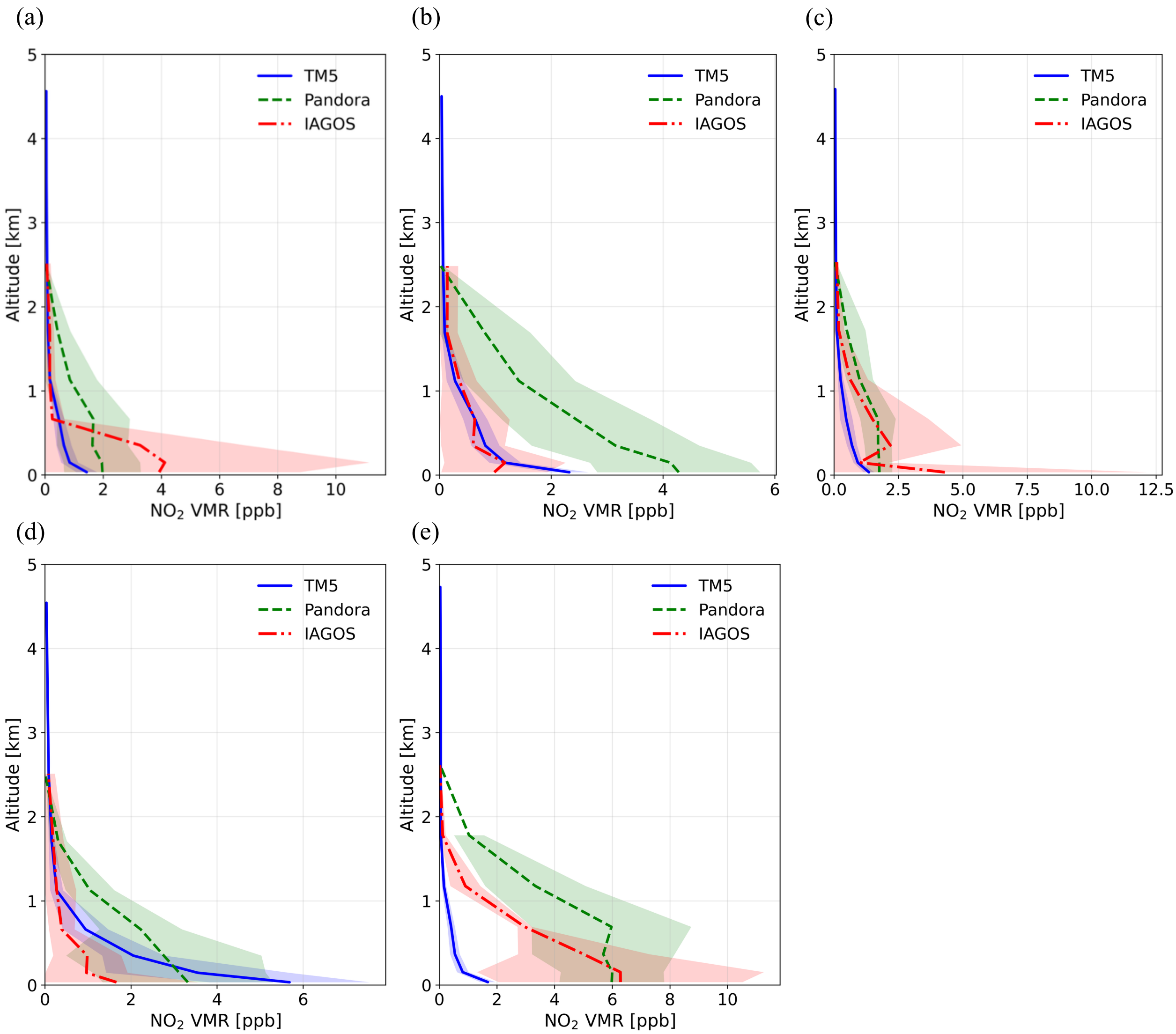


Figure 4. Mean $NO_2$ vertical profiles used for the AMF recalculation at each airport–Pandora pair: (a) FUK, (b) KIX, (c) NRT, (d) ICN, and (e) BKK. Blue, green, and red lines indicate the TM5-MP a priori, Pandora-scaled, and IAGOS-scaled profiles, respectively. Shaded areas indicate the 1σ variability of the matched profiles.

https://doi.org/10.5194/egusphere-2026-4968
Preprint. Discussion started: 11 September 2026


### 4.2 Differences between TM5-MP and observation-scaled $NO_2$ profiles

Figure 4 compares the mean $NO_2$ vertical profiles used for the AMF recalculation at each airport–Pandora pair. The TM5-MP a priori profiles are shown together with the Pandora- and IAGOS-scaled profiles after all profiles were mapped onto the TM5-MP vertical layer structure. The five panels correspond to FUK, KIX, NRT, ICN, and BKK, and the number of matched profiles used at each site is given in each panel. The shaded areas represent the 1σ variability of the matched profiles, providing an indication of how strongly the lower-tropospheric $NO_2$ profile varied during the analysis period. The largest differences among the three profile types appeared in the lower troposphere, mainly below about 3 km. Above this altitude, $NO_2$ mixing ratios were generally small and the differences among the profiles became less pronounced. This vertical pattern indicates that the main uncertainty in the a priori profiles around the airport regions is concentrated near the surface and within the lower troposphere, where local emissions and boundary-layer mixing strongly affect the $NO_2$ distribution. Because the TROPOMI tropospheric $NO_2$ AMF depends on the altitude at which $NO_2$ is located, these lower-tropospheric differences are expected to influence the recalculated AMFs. The comparison also shows that the profile differences were strongly site dependent.

At FUK and NRT, the IAGOS-scaled profiles showed enhanced $NO_2$ in the lowest layers compared with the smoother TM5-MP profiles, suggesting that aircraft observations captured localized lower-tropospheric $NO_2$ enhancements that were not fully represented in the model a priori profiles. At KIX and BKK, the Pandora-scaled profiles indicated relatively elevated $NO_2$ extending through a deeper part of the lower troposphere, implying that the $NO_2$ distribution around the Pandora sites was vertically broader than that represented by TM5-MP. The 1σ ranges were also large at some sites, especially in the lower layers, showing that the observed $NO_2$ profiles varied substantially from case to case.

ICN showed a more complex relationship among the three profiles. The TM5-MP, Pandora-scaled, and IAGOS-scaled profiles differed not only in magnitude but also in their vertical gradients. This behaviour may reflect the combined effects of local emission gradients, differences between the airport and Pandora-site environments, and the limited number of matched IAGOS profiles. Such site-to-site differences suggest that replacing the lower-tropospheric part of the a priori profile does not necessarily produce the same type of AMF response at every airport. Overall, Fig. 4 shows that the TM5-MP a priori profiles do not always reproduce the observation-scaled lower-tropospheric $NO_2$ structure around the selected airport regions. The magnitude and vertical extent of the differences vary by site, but they are consistently most important in the altitude range where aircraft and Pandora observations provide direct constraints. These profile differences provide the physical basis for the AMF changes examined in Sects. 4.3–4.5.

### 4.3 Impact on tropospheric $NO_2$ AMF

Figure 5 compares the operational TROPOMI tropospheric $NO_2$ AMFs with the AMFs recalculated using observation-scaled $NO_2$ profiles. Figure 5(a) shows the results obtained from the IAGOS-scaled profiles after Pandora-time scaling, while Fig. 5(b) shows the results based on the Pandora-scaled profiles. Gray symbols represent individual matched cases, and coloured

https://doi.org/10.5194/egusphere-2026-4968
Preprint. Discussion started: 11 September 2026


symbols with error bars show the site-level means and 1σ variability for each airport–Pandora pair. The 1:1 line indicates the case in which the recalculated AMF is identical to the operational AMF. The recalculated AMFs differed from the operational values, and the direction of the change depended on both the site and the profile used for the recalculation. This behaviour is consistent with the profile differences shown in Fig. 4. Because the tropospheric AMF depends on the vertical placement of $NO_2$, changes in the lower-tropospheric profile can alter the effective sensitivity of the satellite retrieval. When a larger fraction of $NO_2$ is placed closer to the surface, where the retrieval sensitivity is generally lower, the recalculated AMF tends to decrease. For a fixed slant column, this decrease in AMF leads to an increase in the recalculated tropospheric $NO_2$ VCD.

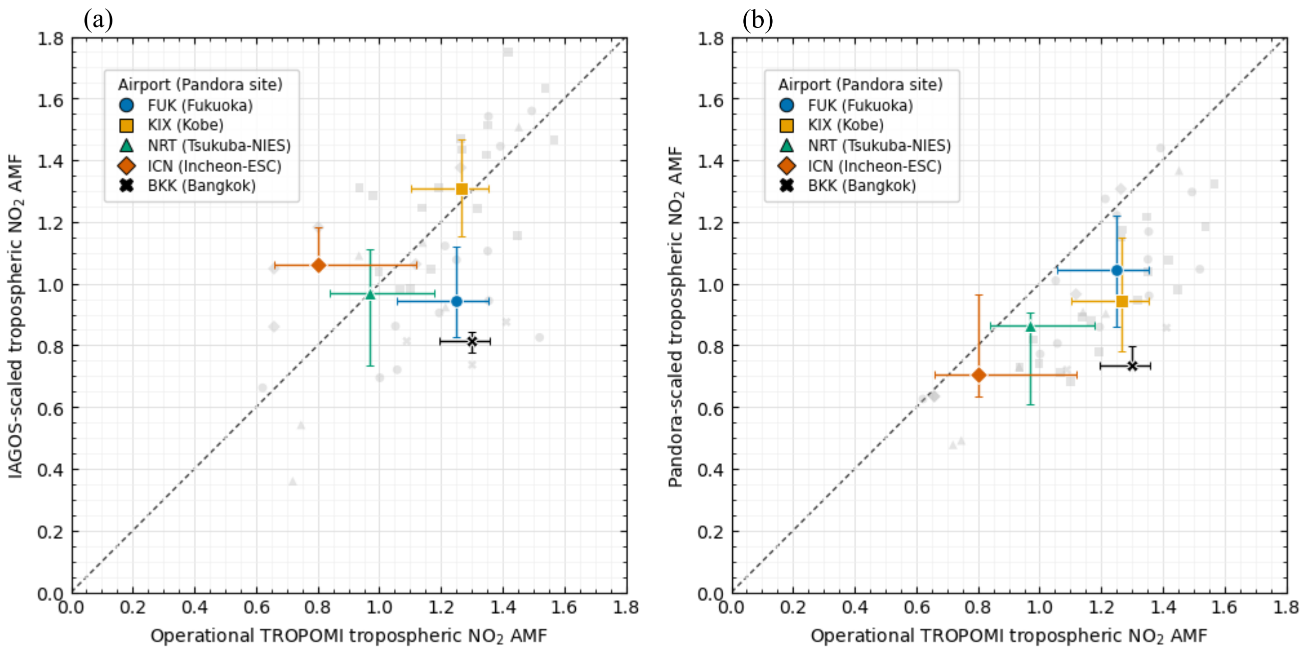


Figure 5. Comparison between operational and recalculated TROPOMI tropospheric $NO_2$ AMFs. (a) AMFs recalculated using the IAGOS-constrained profiles. (b) AMFs recalculated using the Pandora-constrained profiles. Gray symbols indicate individual cases, and coloured symbols with error bars indicate site-level means and 1σ variability for each airport–Pandora pair.

For the IAGOS-scaled case, the site-mean AMFs showed different responses among the airport regions. FUK and BKK AMFs were located below the 1:1 line, indicating that the recalculated values were smaller than the operational values. This is consistent with the enhanced lower-tropospheric $NO_2$ seen in the IAGOS profiles at these sites. In contrast, KIX and ICN AMFs showed recalculated values that were similar to or larger than the operational values, while NRT AMFs were located close to the 1:1 line. These differences indicate that the aircraft-derived lower-tropospheric profile does not introduce a uniform correction across all sites, but rather reflects the site-specific vertical structure observed near each airport.

The Pandora-scaled case showed a more consistent tendency toward lower AMFs. In Fig. 5(b), the site-mean values for most airport–Pandora pairs are located below the 1:1 line, indicating that the Pandora-based profiles generally reduced the AMF relative to the operational retrieval. This suggests that, compared with the TM5-MP a priori profiles, the Pandora-scaled

https://doi.org/10.5194/egusphere-2026-4968
Preprint. Discussion started: 11 September 2026


profiles often placed a larger fraction of $NO_2$ in layers with lower satellite sensitivity. The reduction was particularly clear for BKK and ICN, where the Pandora-scaled AMFs were substantially lower than the operational values.

These results demonstrate that the choice of a priori $NO_2$ vertical profile has a direct impact on the TROPOMI tropospheric $NO_2$ AMF. They also show that IAGOS and Pandora profiles can lead to different AMF responses, even though both provide observation-based constraints. This difference is expected because the IAGOS profiles represent the aircraft descent region near the airport, whereas the Pandora profiles characterize the $NO_2$ vertical distribution around the ground-based site.

### 4.4 Evaluation of recalculated tropospheric $NO_2$ VCDs against Pandora observations

Figure 6 compares Pandora tropospheric $NO_2$ VCDs with the operational and recalculated TROPOMI tropospheric $NO_2$ VCDs. The three panels show the operational product [Fig. 6(a)], the VCDs recalculated using the IAGOS-scaled profiles [Fig. 6(b)], and the VCDs recalculated using the Pandora-scaled profiles [Fig. 6(c)]. The operational TROPOMI product showed a clear low bias relative to Pandora. For the fully matched dataset, the regression slope was well below unity, the MBE was $-2.174 \times 10^{15}$ molec cm$^{-2}$, and only 26.7% of the data points were within the GCOS criterion. This indicates that the operational retrieval tended to underestimate the tropospheric $NO_2$ columns for the airport–Pandora pairs examined here. This low bias is consistent with the profile comparisons in Fig. 4 and the AMF differences in Fig. 5, where the TM5-MP a priori profiles often placed less $NO_2$ in the lower troposphere than did the observation-scaled profiles.

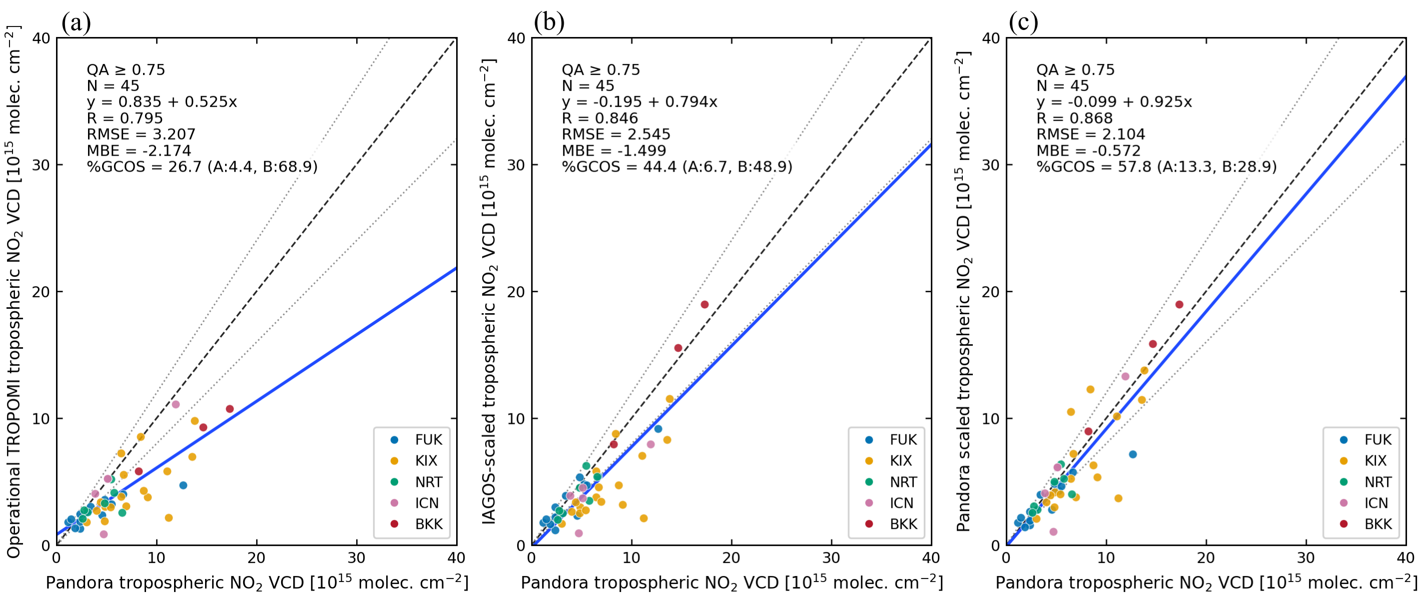


Figure 6. Comparison of Pandora tropospheric $NO_2$ VCDs with (a) operational TROPOMI tropospheric $NO_2$ VCDs, (b) TROPOMI VCDs recalculated using the IAGOS-constrained profiles, and (c) TROPOMI VCDs recalculated using the Pandora-constrained profiles. The black dashed line indicates the 1:1 relationship, the blue solid line represents the linear regression fit, and the dotted lines indicate the GCOS criterion.

https://doi.org/10.5194/egusphere-2026-4968
Preprint. Discussion started: 11 September 2026


Using the IAGOS-scaled profiles reduced this low bias. The correlation coefficient increased from 0.795 to 0.846, while the RMSE decreased from 3.207 to 2.545 × $10^{15}$ molec cm$^{-2}$. The MBE also became less negative, changing from −2.174 to −1.499 × $10^{15}$ molec cm$^{-2}$, and the fraction of data points within the GCOS criterion increased from 26.7 to 44.4%. These changes suggest that replacing the lower part of the a priori profile with aircraft-derived $NO_2$ information can partly correct the low bias in the operational TROPOMI VCDs.

The Pandora-scaled case showed the closest agreement with Pandora observations among the three cases shown in Fig. 6. The correlation coefficient increased to 0.868, the RMSE decreased to 2.104 × $10^{15}$ molec cm$^{-2}$, and the MBE was reduced to −0.572 × $10^{15}$ molec cm$^{-2}$. The percentage of data points within the GCOS criterion also increased to 57.8%. The Pandora-scaled profiles produced VCDs that were closer to those of the Pandora columns. However, this case should be interpreted as a site-scaled sensitivity test rather than as a fully independent evaluation, because the profile information used for the AMF recalculation is taken from the Pandora-site region and is then evaluated against Pandora column observations.

Table 2. Site-level comparison statistics between Pandora tropospheric $NO_2$ VCDs (operational TROPOMI) and operational or IAGOS-recalculated TROPOMI tropospheric $NO_2$ VCDs (IAGOS). Statistics include the number of matched samples (N), Pearson correlation coefficient (R), root-mean-square error (RMSE), mean bias error (MBE), and the percentage of data points within the GCOS criterion.

| Airport | N | R operational / IAGOS | RMSE operational / IAGOS | MBE operational / IAGOS | GCOS (%) operational / IAGOS |
|---|---|---|---|---|---|
| **FUK** | 13 | 0.879 / 0.939 | 2.59 / 1.31 | -1.48 / -0.51 | 15.4 / 53.8 |
| **KIX** | 17 | 0.638 / 0.731 | 3.92 / 3.64 | -3.05 / -2.91 | 17.6 / 17.6 |
| **NRT** | 7 | 0.533 / 0.818 | 1.75 / 1.06 | -1.20 / -0.58 | 42.9 / 71.4 |
| **ICN** | 5 | 0.883 / 0.830 | 1.76 / 2.52 | -0.82 / -1.93 | 80.0 / 40.0 |
| **BKK** | 3 | 1.000 / 1.000 | 5.07 / 1.12 | -4.75 / 0.78 | 0 / 100.0 |

Table 2 summarises the site-level statistics for the operational and IAGOS-recalculated VCDs. The IAGOS-scaled recalculation improved the agreement with Pandora at FUK and NRT. At FUK, R increased from 0.879 to 0.939, the RMSE decreased from 2.59 to 1.31 × $10^{15}$ molec cm$^{-2}$, and the percentage within GCOS increased from 15.4 to 53.8%. At NRT, R increased from 0.533 to 0.818, the RMSE decreased from 1.75 to 1.06 × $10^{15}$ molec cm$^{-2}$, and the percentage within GCOS increased from 42.9 to 71.4%. BKK also showed large apparent improvements, including an RMSE reduction from 5.07 to 1.12 × $10^{15}$ molec cm$^{-2}$ and an increase in the percentage within GCOS from 0 to 100.0%, but this result should be treated cautiously because only three matched samples were available. The response was not uniform across all sites. At KIX, the changes in RMSE and MBE were small, and the percentage within the GCOS criterion remained unchanged. At ICN, the IAGOS-recalculated VCDs showed poorer agreement with Pandora than the operational product, with the RMSE increasing from 1.76 to 2.52 × $10^{15}$ molec cm$^{-2}$ and the percentage within the GCOS criterion decreasing from 80.0 to 40.0%. This does

https://doi.org/10.5194/egusphere-2026-4968
Preprint. Discussion started: 11 September 2026


not necessarily imply that the IAGOS profile itself was less realistic. Rather, it highlights that the aircraft profile represents the airport region, whereas the Pandora column represents conditions around a ground-based site that may be separated from the airport and affected by different local emissions. The small number of matched samples at several sites also means that individual cases can have a strong influence on the site-level statistics.

This site dependence is also consistent with the spatial relationship among the airports, Pandora sites, IAGOS descent tracks, and TROPOMI $NO_2$ fields shown in Fig. 1. At KIX, the strongest $NO_2$ enhancement was located over the Osaka–Kobe urban plume, while the IAGOS descent tracks did not clearly pass through the core of this high-$NO_2$ region. The aircraft-derived profile may therefore have been less representative of the lower-tropospheric $NO_2$ structure influencing the Pandora region, which could explain the limited improvement at this site. A similar interpretation applies to ICN. Although a pronounced $NO_2$ enhancement was present over the broader Seoul–Incheon region, the IAGOS profiles were obtained near the airport and did not appear to sample the main plume directly. In this situation, replacing the lower part of the a priori profile with the aircraft-derived profile can better constrain the airport-region profile, but it does not necessarily improve the agreement with Pandora if the Pandora column is influenced by a different part of the $NO_2$ field.

The sites with improved performance showed a different spatial relationship. At FUK, the airport, Pandora site, and IAGOS tracks were located in a relatively similar local environment, which likely helped the aircraft-derived profile represent the $NO_2$ structure relevant to the comparison. At BKK, the IAGOS descent tracks were located within or close to the main $NO_2$ plume, and the mean wind field suggests transport from the urban plume toward the flight-track region. This spatial correspondence may explain the large apparent improvement after applying the IAGOS-scaled profile, although the small number of matched samples at BKK means that this result should be interpreted cautiously. For NRT, the IAGOS profiles were obtained outside the strongest Tokyo urban plume, in a more suburban or background-like environment. This may have provided a lower-tropospheric profile that was more consistent with the relatively low-$NO_2$ conditions around the airport–Pandora comparison region.

Overall, Fig. 6 and Table 2 show that observation-scaled AMF recalculation can reduce the low bias in TROPOMI tropospheric $NO_2$ VCDs, but the effect is not spatially uniform. The IAGOS-scaled profiles provide direct lower-tropospheric information near airports and can improve the satellite VCDs in several cases. At the same time, the Pandora-based evaluation must be interpreted together with the airport–Pandora representativeness discussed in Sect. 4.1 and the limited number of collocated observations. The aircraft-based $NO_2$ profiles can provide complementary constraints for satellite $NO_2$ AMF calculations, particularly when more collocated profiles become available.

## 5 Discussion

The Pandora-scaled profile recalculation reduced the discrepancy between TROPOMI and Pandora $NO_2$ VCDs, but the recalculated columns did not move to the one-to-one line. We define the Pandora-scaled residual as

$$\text{Pandora-scaled residual} = \text{Pandora-scaled TROPOMI } NO_2 \text{ VCD} - \text{Pandora VCD}. \quad (4)$$

https://doi.org/10.5194/egusphere-2026-4968
Preprint. Discussion started: 11 September 2026


A positive residual indicates that TROPOMI results remain higher than those of Pandora, whereas negative values indicate a residual low bias. For the diagnostic analysis in Fig. 7 and Table 3, we used the absolute Pandora-scaled residual, namely the absolute value of this signed difference. A perfect closure is not expected, because modifying the a priori $NO_2$ profile changes only the AMF calculation and does not constrain the satellite column to the Pandora value. The recalculated VCD still depends on effective tropospheric SCD retrieval by TROPOMI, while the viewing geometry, cloud and surface parameters, and other retrieval inputs remain unchanged.

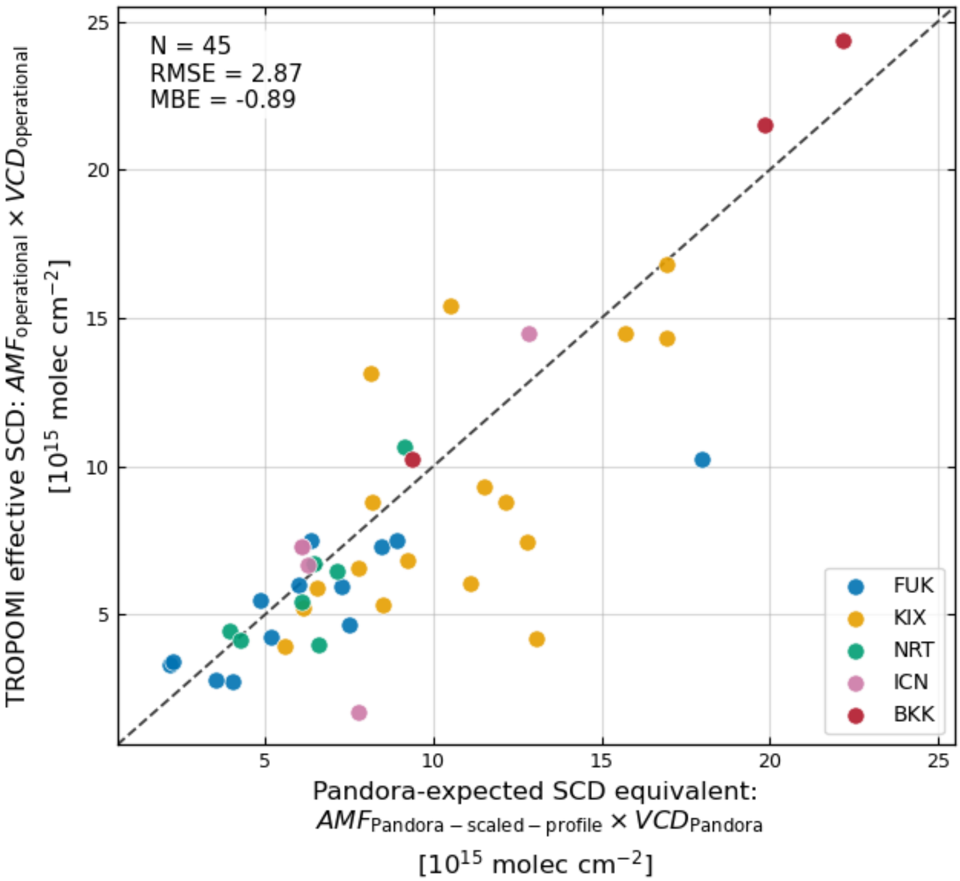


Figure 7. Tropospheric SCD-equivalent closure for Pandora-scaled profile AMF recalculation.

We first examined whether the absolute Pandora-scaled residual was linked to horizontal $NO_2$ variability within the validation area. The coefficient of variation, interquartile range (IQR)-normalized heterogeneity metric, number of QA-filtered pixels, and mean QA value all showed weak relationships with the absolute residuals. Thus, the residual differences were not mainly explained by horizontal heterogeneity within the 10 km sampling area, pixel sampling density, or average retrieval quality. The magnitude of the profile-induced AMF adjustment was also examined. We defined the AMF correction ratio as the Pandora-scaled profile AMF divided by the operational AMF. If the residuals were primarily controlled by the magnitude of

https://doi.org/10.5194/egusphere-2026-4968
Preprint. Discussion started: 11 September 2026


the profile correction, this ratio would be expected to vary systematically with the absolute residual. However, the correlation was weak, indicating that the residual difference is not simply a consequence of applying a larger or smaller AMF correction. This points to additional retrieval-related factors that remain after the profile-dependent part of the AMF has been adjusted.

To examine this point more directly, we used an SCD-equivalent closure analysis. The TROPOMI effective tropospheric SCD was calculated from the product of the operational TROPOMI $NO_2$ VCD and the operational tropospheric AMF. The Pandora-expected SCD-equivalent value was calculated from the Pandora $NO_2$ VCD multiplied by the Pandora-scaled profile AMF. These two quantities express the slant column information implied by the satellite retrieval and by the Pandora reference column under the same Pandora-scaled profile AMF framework. As shown in Fig. 7, they varied in a broadly consistent manner, but they did not follow a one-to-one relationship. Therefore, even when the AMF is recalculated using the Pandora-scaled $NO_2$ profile, a mismatch remains between the TROPOMI effective tropospheric SCD and the SCD-equivalent value expected from Pandora.

This SCD-equivalent mismatch may arise from several sources. Uncertainties in the TROPOMI slant column retrieval, stratosphere–troposphere separation, cloud treatment, surface albedo, and other non-profile AMF inputs can all affect the retrieved column (van Geffen et al., 2020; van Geffen et al., 2022; Latsch et al., 2022). The Pandora reference column also has its own measurement uncertainty and representativeness limitations, especially in regions with strong spatial $NO_2$ gradients. The Pandora-scaled-profile recalculation should therefore be regarded as a sensitivity experiment that isolates the influence of the $NO_2$ vertical profile on the AMF, rather than as a procedure that forces agreement with Pandora.

Overall, Fig. 7 and Table 3 show that the absolute differences remaining after the Pandora-scaled profile recalculation are not primarily controlled by horizontal heterogeneity within the validation radius, pixel sampling density, mean QA value, or magnitude of the AMF correction. The SCD-equivalent closure analysis further shows that replacing the $NO_2$ profile alone cannot remove all differences between TROPOMI and Pandora columns. These results support the use of lower-tropospheric profile information from Pandora and IAGOS as an important constraint on TROPOMI $NO_2$ AMF uncertainty, while also highlighting the need to account for slant column retrieval uncertainty, cloud and surface effects, and spatial representativeness in future retrieval improvements.

Table 3. Correlations between the absolute Pandora-scaled residual and tested sampling or AMF-related metrics. The spatial heterogeneity and associated sampling/quality metrics were evaluated for the 41 samples with at least two QA-filtered TROPOMI pixels within the 10 km validation radius, whereas the AMF correction ratio was calculated for all 45 validation samples.

| **Test metrics** | | **N** | **R** |
|---|---|---|---|
| **Spatial heterogeneity test** | σ / mean | 41 | 0.17 |
| | IQR / median | 41 | 0.12 |
| **Sampling / quality test** | Number of QA-filtered pixels | 41 | −0.17 |
| | Mean QA value | 41 | 0.11 |
| **AMF correction test** | AMF correction ratio | 45 | 0.02 |

https://doi.org/10.5194/egusphere-2026-4968
Preprint. Discussion started: 11 September 2026


## 6 Conclusions

We investigated how lower-tropospheric $NO_2$ profile information affects TROPOMI tropospheric $NO_2$ AMF and VCD calculations near major airports. The analysis combined TROPOMI $NO_2$ observations, Pandora measurements, and IAGOS descent profiles for selected airport–Pandora pairs in Japan, South Korea, and Thailand during March–July 2025. By comparing airport- and Pandora-region TROPOMI $NO_2$ fields, we first assessed whether the Pandora sites could provide a reasonable reference for interpreting $NO_2$ variability near the corresponding airports.

The airport- and Pandora-region TROPOMI $NO_2$ time series generally varied in the same direction, although the absolute $NO_2$ levels often differed between the two regions. This distinction is important for airport validation studies. A nearby Pandora site may capture part of the temporal variability around an airport, but it does not necessarily represent the same mean $NO_2$ environment, especially when the two locations are separated by urban pollutant plumes, coastal gradients, or other local emission features.

Replacing the lower part of the TM5-MP a priori profile with IAGOS- or Pandora-derived $NO_2$ profiles changed the recalculated AMFs mainly through differences in the lower troposphere. The IAGOS profile recalculation reduced the overall low bias of TROPOMI data relative to Pandora and improved several validation statistics, but the effect was not uniform across sites. The improvement was clearer when the aircraft profiles, Pandora site, and satellite-observed $NO_2$ field were spatially consistent. In contrast, the accuracy was limited or degraded when the IAGOS descent profiles sampled an air mass different from that influencing the Pandora column. The Pandora-scaled profile case gave the closest agreement with Pandora, but this case should be regarded as a profile sensitivity test rather than an independent validation.

The residual analysis showed that the remaining differences after the Pandora-scaled-profile recalculation were not mainly controlled by horizontal heterogeneity within the validation radius, pixel sampling density, mean QA value, or magnitude of the AMF correction. The SCD-equivalent closure analysis further showed that modifying the $NO_2$ profile alone cannot fully close the difference between TROPOMI and Pandora columns, because the recalculated VCD still depends on effectively acquired TROPOMI tropospheric SCDs and other non-profile retrieval inputs. These findings show that lower-tropospheric profile information from IAGOS and Pandora can help constrain TROPOMI $NO_2$ AMF uncertainties near airports, while also emphasizing the need to account for slant column retrieval uncertainty, cloud and surface effects, and spatial representativeness in future retrieval improvements.

https://doi.org/10.5194/egusphere-2026-4968
Preprint. Discussion started: 11 September 2026


## Authors' contributions

HL conceptualized the study, developed the main framework and methodology, and wrote the original draft. TF, TS, IS, HT, CM, AP, UB, YuK, YaK, TOS, SSP, MK, YGL, and UK contributed to the methodological development and conceptualization. HT supervised the project and was responsible for project administration. All authors reviewed and edited the manuscript and approved the final version.

## Availability of data and material

The datasets generated in this study are available from the corresponding author upon request. We generated these datasets specifically for the analyses presented in this paper and do not maintain them as an independent data product.

## Competing interests

The authors declare that they have no competing interest.

## Funding

## Acknowledgements

The GOSAT-GW greenhouse gases observing mission is a collaborative project between the Ministry of Environment (MOEJ) and National Institute for Environmental Studies (NIES). The NIES GOSAT-GW project team, along with the research groups at the Earth System Division of NIES, are dedicated to the scientific research and technical developments that are necessary for mission's success, particularly efforts dedicated to the development of Level 2 and higher products.

## References

Berkes, F., Houben, N., Bundke, U., Franke, H., Pätz, H.-W., Rohrer, F., Wahner, A., Petzold, A.: The IAGOS NOx instrument – Design, operation and first results from deployment aboard passenger aircraft, Atmos. Meas. Tech., 11, 3737–3757, https://doi.org/10.5194/amt-11-3737-2018, 2018.

Boersma, K.F., Eskes, H.J., Richter, A., De Smedt, I., Lorente, A., Beirle, S., van Geffen, J.H.G.M., Zara, M., Peters, E., Van Roozendael, M., Wagner, T., Maasakkers, J.D., van der A, R.J., Nightingale, J., De Rudder, A., Irie, H., Pinardi, G., Lambert, J.-C., Compernolle, S.C.: Improving algorithms and uncertainty estimates for satellite NO2 retrievals: Results from the Quality Assurance for Essential Climate Variables (QA4ECV) project, Atmos. Meas. Tech., 11, 6651–6678, https://doi.org/10.5194/amt-11-6651-2018, 2018.

Chan, K.L., Wiegner, M., van Geffen, J., De Smedt, I., Alberti, C., Cheng, Z., Ye, S., Wenig, M.: MAX-DOAS measurements of tropospheric $NO_2$ and HCHO in Munich and the comparison to OMI and TROPOMI satellite observations, Atmos. Meas. Tech., 13, 4499–4520, https://doi.org/10.5194/amt-13-4499-2020, 2020.

Chi, N.D.T., Tanimoto, H., Inomata, S., Fujinawa, T., Müller, A., Sugita, T., Kato, S., Kuze, N., Kanaya, Y., Fujiwara, M., Hirokawa, J., Takashima, H., Nagahama, T., Yamaji, K., Hirokawa, S., Kim, S.-W., Rawat, P., Crawford, J.H.: Characterization of Pandora sky-scan modes from the Japan Pandora Network and evaluation of their use in validating satellite $NO_2$ and HCHO retrievals, ACS ES&T Air 2, 2872–2888, https://doi.org/10.1021/acsestair.5c00223, 2025.

Dimitropoulou, E., Hendrick, F., Pinardi, G., Friedrich, M.M., Merlaud, A., Tack, F., De Longueville, H., Fayt, C., Hermans, C., Laffineur, Q., Fierens, F., Van Roozendael, M.: Validation of TROPOMI tropospheric $NO_2$ columns using dual-scan MAX-DOAS measurements in Uccle, Brussels, Atmos. Meas. Tech., 13, 5165–5191, https://doi.org/10.5194/amt-13-5165-2020, 2020.

Eskes, H.J., Boersma, K.F.: Averaging kernels for DOAS total-column satellite retrievals, Atmos. Chem. Phys., 3, 1285–1291, https://doi.org/10.5194/acp-3-1285-2003, 2003.

Global Climate Observing System (GCOS): Precursors for aerosols and ozone, https://gcos.wmo.int/site/global-climate-observing-system-gcos/essential-climate-variables/precursors-aerosols-and-ozone, last access: 25 June 2026.

Griffin, D., Zhao, X., McLinden, C.A., Boersma, K.F., Bourassa, A., Dammers, E., Degenstein, D., Eskes, H., Fehr, L., Fioletov, V., Hayden, K., Kharol, S.K., Li, S.-M., Makar, P., Martin, R.V.: High-resolution mapping of nitrogen dioxide with TROPOMI: First results and validation over the Canadian oil sands, Geophys. Res. Lett., 46, 1049–1060, https://doi.org/10.1029/2018GL081095, 2019.

Herman, J., Cede, A., Spinei, E., Mount, G., Tzortziou, M., Abuhassan, N.: $NO_2$ column amounts from ground-based Pandora and MFDOAS spectrometers using the direct-sun DOAS technique: Intercomparisons and application to OMI validation, J. Geophys. Res. Atmos., 114, D13307, https://doi.org/10.1029/2009JD011848, 2009.

Ingmann, P., Veihelmann, B., Langen, J., Lamarre, D., Stark, H., Courrèges-Lacoste, G.B.: Requirements for the GMES atmosphere service and ESA's implementation concept: Sentinels-4/-5 and -5p, Remote Sens. Environ., 120, 58–69, https://doi.org/10.1016/j.rse.2012.01.023, 2012.

Judd, L.M., Al-Saadi, J.A., Szykman, J.J., Valin, L.C., Janz, S.J., Kowalewski, M.G., Eskes, H.J., Veefkind, J.P., Cede, A., Mueller, M., Gebetsberger, M., Swap, R., Pierce, R.B., Nowlan, C.R., Abad, G.G., Nehrir, A., Williams, D.: Evaluating Sentinel-5P TROPOMI tropospheric $NO_2$ column densities with airborne and Pandora spectrometers near New York City and Long Island Sound, Atmos. Meas. Tech., 13, 6113–6140, https://doi.org/10.5194/amt-13-6113-2020, 2020.

Kim, J., Jeong, U., Ahn, M.-H., Kim, J.H., Park, R.J., Lee, H., Song, C.H., Choi, Y.-S., Lee, K.-H., Yoo, J.-M., Jeong, M.-J., Park, S.K., Lee, K.-M., Song, C.K., Kim, S.-W., Kim, Y.J., Kim, S.-K., Kim, M., Go, S., Liu, X., Chance, K., Miller, C.C., Al-Saadi, J., Veefkind, P., Levelt, P.F., Edwards, D.P., Kang, M., Eo, M., Bak, J., Baek, K., Kwon, H.-A., Park, J., Chong, H., Cha, Y., Lee, K., Choi, H., Lee, S., Choi, M., Cho, C.: New era of air quality monitoring from space: Geostationary Environment Monitoring Spectrometer (GEMS), Bull. Am. Meteorol. Soc., 101, E1–E22, https://doi.org/10.1175/BAMS-D-18-0013.1, 2020.

Krotkov, N.A., McLinden, C.A., Li, C., Lamsal, L.N., Celarier, E.A., Marchenko, S.V., Swartz, W.H., Bucsela, E.J., Joiner, J., Duncan, B.N., Boersma, K.F., Veefkind, J.P., Levelt, P.F., Fioletov, V.E., Dickerson, R.R., He, H., Lu, Z., Streets, D.G.:

Aura OMI observations of regional $SO_2$ and $NO_2$ pollution changes from 2005 to 2015, Atmos. Chem. Phys., 16, 4605–4629, https://doi.org/10.5194/acp-16-4605-2016, 2016.

Lange, K., Richter, A., Schönhardt, A., Meier, A. C., Bösch, T., Seyler, A., Krause, K., Behrens, L. K., Wittrock, F., Merlaud, A., Tack, F., Fayt, C., Friedrich, M. M., Dimitropoulou, E., Van Roozendael, M., Kumar, V., Donner, S., Dörner, S., Lauster, B., Razi, M., Borger, C., Uhlmannsiek, K., Wagner, T., Ruhtz, T., Eskes, H., Bohn, B., Santana Diaz, D., Abuhassan, N., Schüttemeyer, D., and Burrows, J. P.: Validation of Sentinel-5P TROPOMI tropospheric NO2 products by comparison with NO2 measurements from airborne imaging DOAS, ground-based stationary DOAS, and mobile car DOAS measurements during the S5P-VAL-DE-Ruhr campaign, Atmos. Meas. Tech., 16, 1357–1389, https://doi.org/10.5194/amt-16-1357-2023, 2023.

Latsch, M., Richter, A., Eskes, H., Sneep, M., Wang, P., Veefkind, P., Lutz, R., Loyola, D., Argyrouli, A., Valks, P., Wagner, T., Sihler, H., van Roozendael, M., Theys, N., Yu, H., Siddans, R., and Burrows, J. P.: Intercomparison of Sentinel-5P TROPOMI cloud products for tropospheric trace gas retrievals, Atmos. Meas. Tech., 15, 6257–6283, https://doi.org/10.5194/amt-15-6257-2022, 2022.

Lim, H., Tanimoto, H., Fujinawa, T., Sugita, T., Kanaya, Y., Kasai, Y., Sato, T., Park, S., Kim, M., Kim, S., Shimizu, A., Morino, I.: Refining $NO_2$ air-mass factors with scattering clouds: TROPOMI-based assessment in TANSO-3/GOSAT-GW data processing, Remote Sens. Lett., 17, 841–852, https://doi.org/10.1080/2150704X.2026.2673539, 2026.

Lin, J.-T., Liu, M., Xin, J., Boersma, K.F., Spurr, R., Martin, R.V., Zhang, Q.: Influence of aerosols and surface reflectance on satellite $NO_2$ retrieval: Seasonal and spatial characteristics and implications for $NO_x$ emission constraints, Atmos. Chem. Phys., 14, 1441–1461, https://doi.org/10.5194/acp-14-1441-2014, 2014.

Lin, J.-T., Liu, M., Xin, J., Boersma, K.F., Spurr, R., Martin, R.V., Zhang, Q.: Influence of aerosols and surface reflectance on satellite $NO_2$ retrieval: Seasonal and spatial characteristics and implications for $NO_x$ emission constraints, Atmos. Chem. Phys., 15, 11217–11241, https://doi.org/10.5194/acp-15-11217-2015, 2015.

Liu, M., Lin, J., Boersma, K.F., Pinardi, G., Wang, Y., Chimot, J., Wagner, T., Xie, P., Eskes, H., Van Roozendael, M., Hendrick, F., Wang, P., Wang, T., Yan, Y., Chen, L., Ni, R.: Improved aerosol correction for OMI tropospheric $NO_2$ retrieval over East Asia: Constraint from CALIOP aerosol vertical profile, Atmos. Meas. Tech., 12, 1–21, https://doi.org/10.5194/amt-12-1-2019, 2019.

Liu, M., Lin, J., Wang, Y., Sun, Y., Zheng, B., Shao, J., Chen, L., Zheng, Y., Chen, J., Fu, T.-M., Yan, Y., Zhang, Q.: A new TROPOMI product for tropospheric $NO_2$ columns over East Asia with explicit aerosol corrections, Atmos. Meas. Tech., 13, 4247–4259, https://doi.org/10.5194/amt-13-4247-2020, 2020.

Liu, S., Valks, P., Pinardi, G., Xu, J., Chan, K. L., Argyrouli, A., Lutz, R., Beirle, S., Khorsandi, E., Baier, F., Huijnen, V., Bais, A., Donner, S., Dörner, S., Gratsea, M., Hendrick, F., Karagkiozidis, D., Lange, K., Piters, A. J. M., Remmers, J., Richter, A., Van Roozendael, M., Wagner, T., Wenig, M., and Loyola, D. G.: An improved TROPOMI tropospheric NO2 research product over Europe, Atmos. Meas. Tech., 14, 7297–7327, https://doi.org/10.5194/amt-14-7297-2021, 2021.

Lorente, A., Boersma, K.F., Yu, H., Dörner, S., Hilboll, A., Richter, A., Liu, M., Lamsal, L.N., Barkley, M., De Smedt, I., Van Roozendael, M., Wang, Y., Wagner, T., Beirle, S., Lin, J.-T., Krotkov, N.A., Stammes, P., Wang, P., Eskes, H.J., Krol, M.C.: Structural uncertainty in air mass factor calculation for NO2 and HCHO satellite retrievals, Atmos. Meas. Tech., 10, 759–782, https://doi.org/10.5194/amt-10-759-2017, 2017.

https://doi.org/10.5194/egusphere-2026-4968
Preprint. Discussion started: 11 September 2026


Monks, P.S., Archibald, A.T., Colette, A., Cooper, O., Coyle, M., Derwent, R., Fowler, D., Granier, C., Law, K.S., Mills, G.E., Stevenson, D.S., Tarasova, O., Thouret, V., von Schneidemesser, E., Sommariva, R., Wild, O., Williams, M.L.: Tropospheric ozone and its precursors from the urban to the global scale from air quality to short-lived climate forcer, Atmos. Chem. Phys., 15, 8889–8973, https://doi.org/10.5194/acp-15-8889-2015, 2015.

Mouat, A.P., Spinei, E., Kaiser, J.: Informing near-airport satellite $NO_2$ retrievals using Pandora sky-scanning observations, ACS ES&T Air, 1, 1617–1628, https://doi.org/10.1021/acsestair.4c00158, 2024.

Palmer, P.I., Jacob, D.J., Chance, K., Martin, R.V., Spurr, R.J.D., Kurosu, T.P., Bey, I., Yantosca, R., Fiore, A.M., Li, Q.: Air mass factor formulation for spectroscopic measurements from satellites: Application to formaldehyde retrievals from the Global Ozone Monitoring Experiment, J. Geophys. Res. Atmos., 106, 14539–14550, https://doi.org/10.1029/2000JD900772, 2001.

Petzold, A., Thouret, V., Gerbig, C., Zahn, A., Brenninkmeijer, C.A.M., Gallagher, M., Hermann, M., Pontaud, M., Ziereis, H., Boulanger, D., Marshall, J., Nédélec, P., Smit, H., Friess, U., Flaud, J-M., Wahner, A., Cammas, J-P., Volz-Thomas, A., IAGOS Team.: Global-scale atmosphere monitoring by in-service aircraft: Current achievements and future prospects of IAGOS, Tellus B Chem. Phys. Meteorol., 67, 28452, https://doi.org/10.3402/tellusb.v67.28452, 2015.

Rawat, P., Crawford, J. H., Travis, K. R., Judd, L. M., Demetillo, M. A. G., Valin, L. C., Szykman, J. J., Whitehill, A., Baumann, E., and Hanisco, T. F.: Maximizing the scientific application of Pandora column observations of HCHO and NO2, Atmos. Meas. Tech., 18, 2899–2917, https://doi.org/10.5194/amt-18-2899-2025, 2025.

Riess, T. C. V. W., Boersma, K. F., Van Roy, W., de Laat, J., Dammers, E., and van Vliet, J.: To new heights by flying low: comparison of aircraft vertical NO2 profiles to model simulations and implications for TROPOMI NO2 retrievals, Atmos. Meas. Tech., 16, 5287–5304, https://doi.org/10.5194/amt-16-5287-2023, 2023.

Tack, F., Merlaud, A., Iordache, M.-D., Pinardi, G., Dimitropoulou, E., Eskes, H., Bomans, B., Veefkind, P., and Van Roozendael, M.: Assessment of the TROPOMI tropospheric NO2 product based on airborne APEX observations, Atmos. Meas. Tech., 14, 615–646, https://doi.org/10.5194/amt-14-615-2021, 2021.

van Geffen, J., Boersma, K.F., Eskes, H., Sneep, M., ter Linden, M., Zara, M., Veefkind, J.P.: S5P TROPOMI $NO_2$ slant column retrieval: Method, stability, uncertainties and comparisons with OMI, Atmos. Meas. Tech., 13, 1315–1335, https://doi.org/10.5194/amt-13-1315-2020, 2020.

van Geffen, J., Eskes, H., Compernolle, S., Pinardi, G., Verhoelst, T., Lambert, J.-C., Sneep, M., ter Linden, M., Ludewig, A., Boersma, K.F., Veefkind, J.P.: Sentinel-5P TROPOMI $NO_2$ retrieval: Impact of version v2.2 improvements and comparisons with OMI and ground-based data, Atmos. Meas. Tech., 15, 2037–2060, https://doi.org/10.5194/amt-15-2037-2022, 2022.

van Geffen, J.H.G.M., Eskes, H.J., Boersma, K.F., Maasakkers, J.D., Veefkind, J.P.: TROPOMI ATBD of the total and tropospheric $NO_2$ data products, issue 2.8.0. S5P-KNMI-L2-0005-RP, Royal Netherlands Meteorological Institute, De Bilt: https://sentiwiki.copernicus.eu/web/s5p-documents, last access: 25 June 2026.

Veefkind, J.P., Aben, I., McMullan, K., Förster, H., de Vries, J., Otter, G., Claas, J., Eskes, H.J., de Haan, J.F., Kleipool, Q., van Weele, M., Hasekamp, O., Hoogeveen, R., Landgraf, J., Snel, R., Tol, P.J.J., Ingmann, P., Voors, R., Kruizinga, B., Vink, R., Visser, H., Levelt, P.F.: TROPOMI on the ESA Sentinel-5 Precursor: A GMES mission for global observations of the atmospheric composition for climate, air quality and ozone layer applications, Remote Sens. Environ., 120, 70–83, https://doi.org/10.1016/j.rse.2011.09.027, 2012.

https://doi.org/10.5194/egusphere-2026-4968
Preprint. Discussion started: 11 September 2026


Verhoelst, T., Compernolle, S., Pinardi, G., Lambert, J.-C., Eskes, H. J., Eichmann, K.-U., Fjæraa, A. M., Granville, J., Niemeijer, S., Cede, A., Tiefengraber, M., Hendrick, F., Pazmiño, A., Bais, A., Bazureau, A., Boersma, K. F., Bognar, K., Dehn, A., Donner, S., Elokhov, A., Gebetsberger, M., Goutail, F., Grutter de la Mora, M., Gruzdev, A., Gratsea, M., Hansen, G. H., Irie, H., Jepsen, N., Kanaya, Y., Karagkiozidis, D., Kivi, R., Kreher, K., Levelt, P. F., Liu, C., Müller, M., Navarro Comas, M., Piters, A. J. M., Pommereau, J.-P., Portafaix, T., Prados-Roman, C., Puentedura, O., Querel, R., Remmers, J., Richter, A., Rimmer, J., Rivera Cárdenas, C., Saavedra de Miguel, L., Sinyakov, V. P., Stremme, W., Strong, K., Van Roozendael, M., Veefkind, J. P., Wagner, T., Wittrock, F., Yela González, M., and Zehner, C.: Ground-based validation of the Copernicus Sentinel-5P TROPOMI NO2 measurements with the NDACC ZSL-DOAS, MAX-DOAS and Pandonia global networks, Atmos. Meas. Tech., 14, 481–510, https://doi.org/10.5194/amt-14-481-2021, 2021.

Williams, J.E., Boersma, K.F., Le Sager, P., Verstraeten, W.W.: The high-resolution version of TM5-MP for optimized satellite retrievals: Description and validation, Geosci. Model Dev., 10, 721–750, https://doi.org/10.5194/gmd-10-721-2017, 2017.

Zoogman, P., Liu, X., Suleiman, R.M., Pennington, W.F., Flittner, D.E., Al-Saadi, J.A., Hilton, B.B., Nicks, D.K., Newchurch, M.J., Carr, J.L., Janz, S.J., Andraschko, M.R., Arola, A., Baker, B.D., Canova, B.P., Chan Miller, C., Cohen, R.C., Davis, J.E., Dussault, M.E., Edwards, D.P., Fishman, J., Ghulam, A., González Abad, G., Grutter, M., Herman, J.R., Houck, J., Jacob, D.J., Joiner, J., Kerridge, B.J., Kim, J., Krotkov, N.A., Lamsal, L., Li, C., Lindfors, A.V., Martin, R.V., McElroy, C.T., McLinden, C.A., Natraj, V., Neil, D.O., Nowlan, C.R., O'Sullivan, E.J., Palmer, P.I., Pierce, R.B., Pippin, M.R., Saiz-Lopez, A., Spurr, R.J.D., Szykman, J.J., Torres, O., Veefkind, J.P., Veihelmann, B., Wang, H., Wang, J., Chance, K.: Tropospheric emissions: monitoring of pollution (TEMPO), J. Quant. Spectrosc. Radiat. Transf., 186, 17–39, https://doi.org/10.1016/j.jqsrt.2016.05.008, 2017.